



RESEARCH ARTICLE | MARCH 22 2019

Simultaneously improved sensitivity and response speed of $\beta\text{-Ga}_2\text{O}_3$ solar-blind photodetector via localized tuning of oxygen deficiency

L. X. Qian ; H. Y. Liu; H. F. Zhang ; Z. H. Wu; W. L. Zhang*Appl. Phys. Lett.* 114, 113506 (2019)<https://doi.org/10.1063/1.5088665>

Articles You May Be Interested In

$\beta\text{-Ga}_2\text{O}_3$ solar-blind deep-ultraviolet photodetector based on a four-terminal structure with or without Zener diodes

AIP Advances (April 2016)

Solar blind Schottky photodiode based on an MOCVD-grown homoepitaxial $\beta\text{-Ga}_2\text{O}_3$ thin film

APL Mater. (February 2019)

High-performance $\alpha\text{-Ga}_2\text{O}_3$ solar-blind photodetectors by pulsed magnetron sputtering deposition

J. Vac. Sci. Technol. A (March 2024)



Applied Physics Letters

Special Topics Open for Submissions

[Learn More](#)

Simultaneously improved sensitivity and response speed of β -Ga₂O₃ solar-blind photodetector via localized tuning of oxygen deficiency

Cite as: Appl. Phys. Lett. **114**, 113506 (2019); doi: [10.1063/1.5088665](https://doi.org/10.1063/1.5088665)

Submitted: 13 January 2019 · Accepted: 10 March 2019 ·

Published Online: 22 March 2019



View Online



Export Citation



CrossMark

L. X. Qian,^{1,a)} H. Y. Liu,¹ H. F. Zhang,² Z. H. Wu,³ and W. L. Zhang¹

AFFILIATIONS

¹State Key Laboratory of Electronic Thin Films and Integrated Devices, School of Electronic Science and Engineering, University of Electronic Science and Technology of China, Chengdu 611731, China

²Photonics Laboratory, King Abdullah University of Science and Technology, Thuwal 23955-6900, Saudi Arabia

³Department of Applied Physics, The Hong Kong Polytechnic University, Hung Hom, Kowloon, Hong Kong

^{a)}Author to whom correspondence should be addressed: lxqian@uestc.edu.cn

ABSTRACT

Recently, β -Ga₂O₃ solar-blind photodetectors (PDs) have been extensively investigated for a wide range of civil and military applications. Among them, the metal-semiconductor-metal (MSM) structure is one of the most popular candidates due to the merits of fabrication simplicity, the need for only one single-dopant active layer, easy integration with readout circuitry, high quantum efficiency, *etc.* However, there is generally a tradeoff between sensitivity and response speed due to the specific internal gain mechanism. In this work, MSM PDs based on the molecular beam epitaxy-grown β -Ga₂O₃ film were fabricated, and the metal/semiconductor (M/S) interfacial properties were tailored through the low-energy Ar-plasma pretreatment, resulting in the localized oxygen deficiency and a sharper interface. Accordingly, the PD sensitivity was dramatically improved, and the advantage of internal gain, *i.e.*, high quantum efficiency, was preserved or became even larger. For example, the 60-W pretreated sample exhibited a high responsivity (*R*) of 8.41 A/W and a large specific detectivity (*D*^{*}) of 1.24×10^{14} Jones, both increasing by one order of magnitude in comparison with the untreated sample. More interestingly, the response speed was unexpectedly accelerated, which is ascribed to the rapid and direct tunneling of electrons at the M/S interface as well as to the reduction in RC time constant based on the data analysis and the underlying physical principle discussion. The treatment conditions can be further optimized to counterbalance some side effects. These findings reveal an efficient technique for comprehensively improving the performance of β -Ga₂O₃ solar-blind PDs.

Published under license by AIP Publishing. <https://doi.org/10.1063/1.5088665>

Ultraviolet (UV) light is divided into four spectral bands: UV-A (400–320 nm), UV-B (320–280 nm), UV-C (280–200 nm), and vacuum UV (200–10 nm). Among them, the UV-C light from solar radiation cannot reach the Earth's surface due to its absorption by the stratospheric ozone layer and thus is also named as solar-blind UV. This feature provides an extremely low natural background for solar-blind photodetection and is beneficial for a wide range of applications, *e.g.*, flame detection, non-line-of-sight optical communication, and missile warning.¹ The solar-blind photodetectors (PDs) based on wide-bandgap semiconductors are promising candidates because of their small size, light weight, and low power consumption.^{2–5} Particularly, β -Ga₂O₃ possesses an intrinsic bandgap of ~ 4.9 eV and so is naturally suitable for solar-blind photodetection without the need for any alloying processes, which makes β -Ga₂O₃ PDs a better

alternative, and therefore have been extensively explored very recently.^{6–9} Among various PD structures, the metal-semiconductor-metal (MSM) one is an attractive candidate due to its fabrication simplicity, the need for only one single-dopant active layer, easy integration with readout circuitry, and low parasitic capacitance.^{10,11} Moreover, MSM PD typically exhibits high responsivity, which is a critical merit especially for detecting extremely weak signals.¹ It is owing to the presence of internal gain, which often originates from photo-generated minor-carrier trapping by deep-level states.^{12,13} In the case of β -Ga₂O₃, these traps are most likely a combination of the metal/semiconductor (M/S) interface and bulk states associated with oxygen vacancies (*V*_o's), which often impact the material properties and the PD performance significantly.^{14,15} The sweep-out and re-injection of electrons to maintain charge neutrality lead to the

generation of multiple electrons per collected photon and subsequent high quantum efficiency.^{16,17} However, the carrier trapping/detrapping processes are relatively slow, which degrades the response speed,^{18,19} that is, the so-called persistent photoconductivity (PPC).²⁰ Hence, there is often a tradeoff between sensitivity and response speed. For example, the *in situ* annealing in oxygen effectively reduced the V_o 's in the β -Ga₂O₃ film, and thus accelerated the response speed of MSM PD. However, much smaller photocurrent (4 nA) was achieved than that with the as-grown β -Ga₂O₃ (122 nA), suggesting great lower responsivity.²¹ The weakened internal gain mechanism due to the passivation of V_o -related traps could be responsible for the degraded sensitivity besides the establishment of Schottky contacts. Similarly, Cui *et al.* comparably investigated the MSM PDs based on sputtering-deposited amorphous Ga₂O₃ films. The decay time was apparently shortened from $1.48 \times 10^6 \mu\text{s}$ to $19.10 \mu\text{s}$ with increasing oxygen flux from 0 sccm to 0.14 sccm. Nevertheless, the responsivity was dramatically degraded from 91.88 A/W to 0.19 A/W, which can also be attributed to the suppressed V_o -related carrier trapping and the subsequent loss of internal gain.¹³ These findings were confirmed in the In-doped Ga₂O₃ MSM PDs as well.¹⁰ Clearly, the approaches to simply passivate the V_o -related traps in Ga₂O₃ as a whole are very effective in solving the PPC issue, but risk sacrificing one of the most prominent merits, high sensitivity, in MSM PDs.

In this work, the MSM PDs based on a molecular beam epitaxy (MBE)-grown β -Ga₂O₃ film were fabricated, and the low-energy Ar-plasma pretreatment was conducted selectively on the area underneath contacts. The experimental results show that both sensitivity and response speed can be simultaneously improved through this approach, and the inner physical mechanisms are discussed in depth.

The out-of-plane X-ray diffraction (XRD) curves and the optical transmission spectra (supplementary material, Figs. S1 and S2, respectively) demonstrate a single-phase structure with (201) preferred orientation and an optical bandgap of 4.92 eV for our prepared β -Ga₂O₃ films. As shown in Fig. 1, the β -Ga₂O₃ area without the cover of photoresist was exposed to the Ar plasma for 5 min before metal

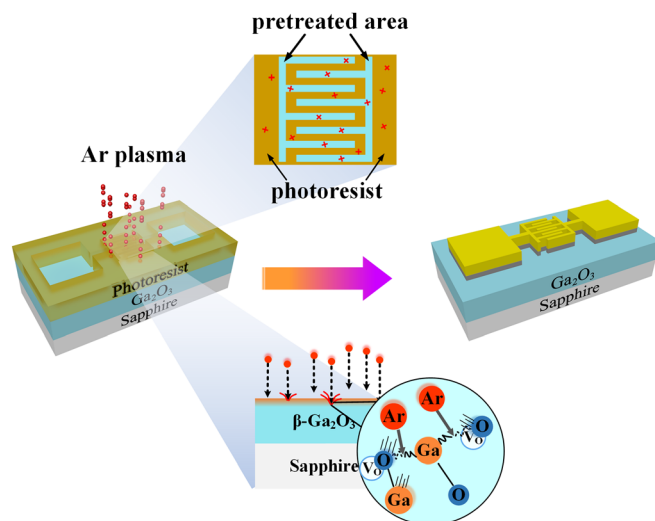


FIG. 1. Schematic diagrams of the selective Ar-plasma pretreatment on the β -Ga₂O₃ MSM PD.

deposition, using a reactive-ion-etching system with different radio frequency (RF) powers, i.e., 30 W and 60 W, respectively. The PD without pretreatment was also prepared as the control sample. Then, the samples herein are referred to as sample-ctrl, sample-30, and sample-60. The details on device fabrication and measurements are introduced in supplementary material S1 and S2.

The atomic force microscopy (AFM) images (supplementary material, Fig. S3) indicate that the surface of treated samples became much smoother than that of sample-ctrl. The surface polishing was attributed to the ion-bombardment effect during Ar-plasma pretreatment, which was more effective under milder conditions, i.e., plasma-generating power of 30 W. Ion bombardment can break the weak chemical bonds by atom collision and transfer the kinetic energy to the atoms for network reconstruction at the material surface.²²

Each X-ray photoelectron spectroscopy (XPS) O 1s spectrum can be resolved into three components based on Gaussian fitting analysis [Fig. 2(a)], which are centered at (1) 530.6 eV (O_I), related to the O^{2-} ions without surrounding V_o 's; (2) 531.2 eV (O_{II}), characterizing the O^{2-} ions in oxygen-deficient regions; and (3) 532.1 eV (O_{III}), corresponding to the chemisorbed species.²³ The intensity ratio of $O_{II}/(O_I + O_{II})$ is $\sim 4\%$ for sample-ctrl, which indicates that the as-prepared MBE-grown β -Ga₂O₃ film had good stoichiometry. With the Ar-plasma treatment, they were dramatically increased to 12.8% and 18.5% for sample-30 and sample-60, respectively, suggesting the appearance of more V_o 's. This observation is also confirmed by the spectra after the 5-s etching [Fig. 2(b)]. It was reported that energetic Ar ion bombardment during plasma exposure can lead to the preferential sputtering of the relatively light atoms from II-VI or III-V group semiconductors, e.g., oxygen in ZnO or nitrogen in GaN, as a result of the momentum transfers during physical collisions.^{24–26} In our case, the increase in V_o 's in β -Ga₂O₃ can be attributed to the preferential dissociation of oxygen atoms by collisions as illustrated in Fig. 1.

As shown in Figs. 3(a) and 3(b), both dark current (I_{dark}) and photocurrent (I_{photo}) were significantly increased by the pretreatment,

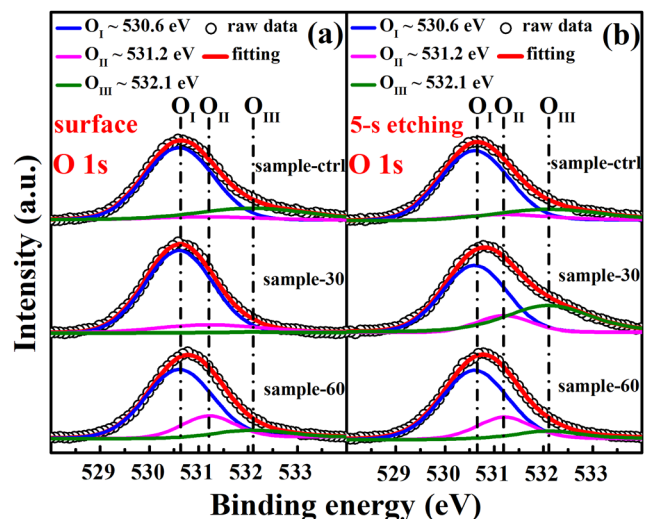


FIG. 2. XPS O 1s core-level spectra of β -Ga₂O₃ films: (a) at the surface and (b) after the 5-s etching.

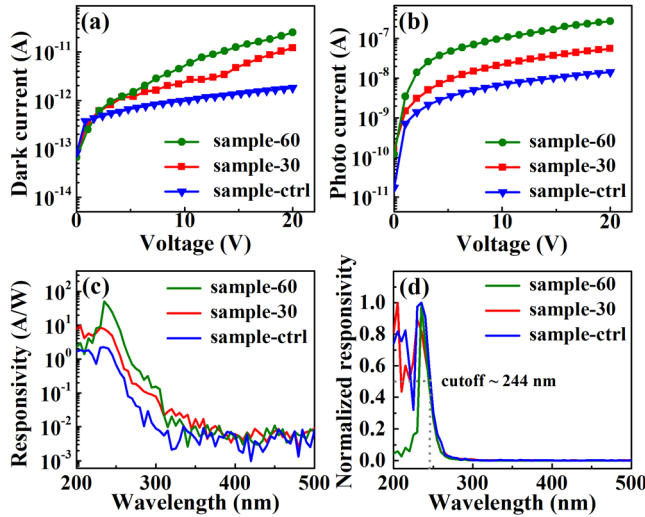


FIG. 3. Semi-logarithmic current-voltage (*I*-*V*) plots of the β -Ga₂O₃ MSM PDs characterized (a) in the dark and (b) under 254-nm and 34.7- μ W/cm² illumination; (c) semi-logarithmic and (d) normalized spectral response under a 10-V bias.

which was more prominent for higher plasma-generating power. As listed in Table I, the increased responsivity reveals the dramatically improved sensitivity. D^* is another key figure-of-merit, which describes the sensitivity considering not only the photo-response but also the noise floor, and is expressed as

$$D^* = R \sqrt{\frac{S}{2qI_{\text{dark}}}}, \quad (1)$$

where S is the effective illumination area, with the shot noise from I_{dark} regarded as the major contribution to the noise floor.²⁷ It was found that sample-60 exhibits the highest D^* (i.e., 1.24×10^{14} Jones), about one order of magnitude higher than that of sample-ctrl. However, if the plasma exposure time is prolonged to 15 min, an obvious loss in D^* appeared due to the dramatically increased I_{dark} , whose impact is too large to be offset by the increase in R (supplementary material, Fig. S4). Moreover, the Ar-plasma pretreated samples possess much higher responsivity than sample-ctrl throughout the whole solar-blind region, which is more apparent for sample-60 [Fig. 3(c)]. The -3-dB cutoff wavelengths are all about 244 nm for three samples [Fig. 3(d)], revealing that the Ar-plasma treatment does not introduce enough subgap states as far as the whole bulk β -Ga₂O₃ is concerned.

For a more detailed investigation, the XPS depth-profile analysis with the etching rate of ~ 0.25 nm/s was also conducted as shown in Fig. 4. It was found that the intensity ratio of $O_{II}/(O_I + O_{II})$ in

TABLE I. Summary of the key parameters for different samples under a bias of 10 V.

	R (A/W)	D^* (Jones)	T_r/T_d (s)	τ_{r1}/τ_{r2} (s)	τ_{d1}/τ_{d2} (s)
Sample-ctrl	0.49	1.63×10^{13}	26.2/2.7	9.19/36.98	0.63/7.39
Sample-30	1.74	3.82×10^{13}	6.3/1.1	3.27/35.27	0.47/9.87
Sample-60	8.41	1.24×10^{14}	18.0/1.6	2.97/41.22	0.41/12.23

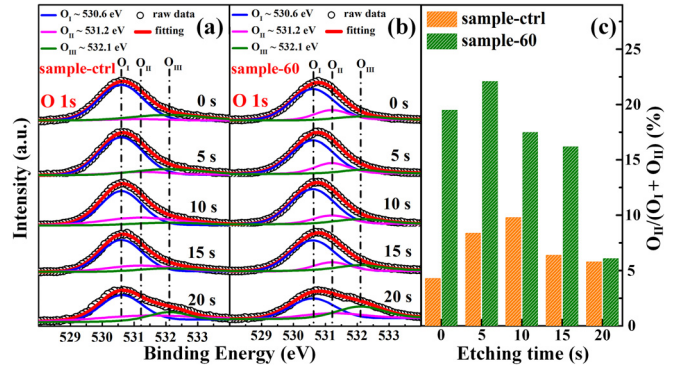


FIG. 4. XPS O 1s core-level spectra with respect to depth: (a) sample-ctrl and (b) sample-60; (c) histogram of $O_{II}/(O_I + O_{II})$ for sample-ctrl and sample-60.

sample-60 decreases rapidly from the etching time of 5 s to 20 s, at which it reaches the baseline level of sample-ctrl. That is, our Ar-plasma pretreatment only impacted the near surface region of the β -Ga₂O₃ film (~ 5 nm deep), which should be attributed to the relatively low ion energies. Moreover, the pretreatment was performed selectively on the area underneath contacts, not including that between them; V_o 's act as donor states in β -Ga₂O₃. Therefore, an ultrathin and highly conductive layer was formed between the contact and the bulk β -Ga₂O₃, which lowered the effective barrier height at the interface, thus facilitating the direct tunneling of electrons in the electric field (Fig. 5). Moreover, a sharper M/S interface due to surface polishing of the β -Ga₂O₃ film might further contribute to this effect. Hence, the observed increases in both I_{dark} and I_{photo} can be ascribed to the reduction of contact rather than bulk resistance with selective Ar-plasma pretreatment.²⁵ In addition, it is believed that more hole trapping at the M/S interface due to increased localized oxygen deficiency could also contribute higher internal gain, and accordingly larger I_{photo} .

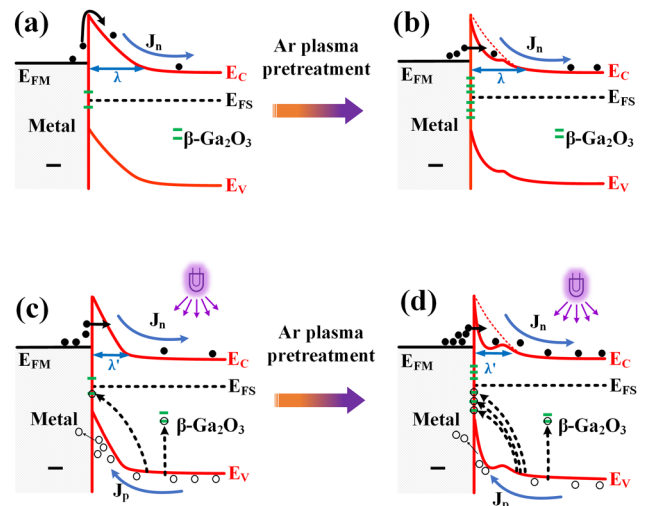


FIG. 5. Schematic energy band diagram of the β -Ga₂O₃ MSM PDs: (a) without and (b) with Ar-plasma pretreatment in the dark; (c) without and (d) with the Ar-plasma pretreatment under UV-C illumination.

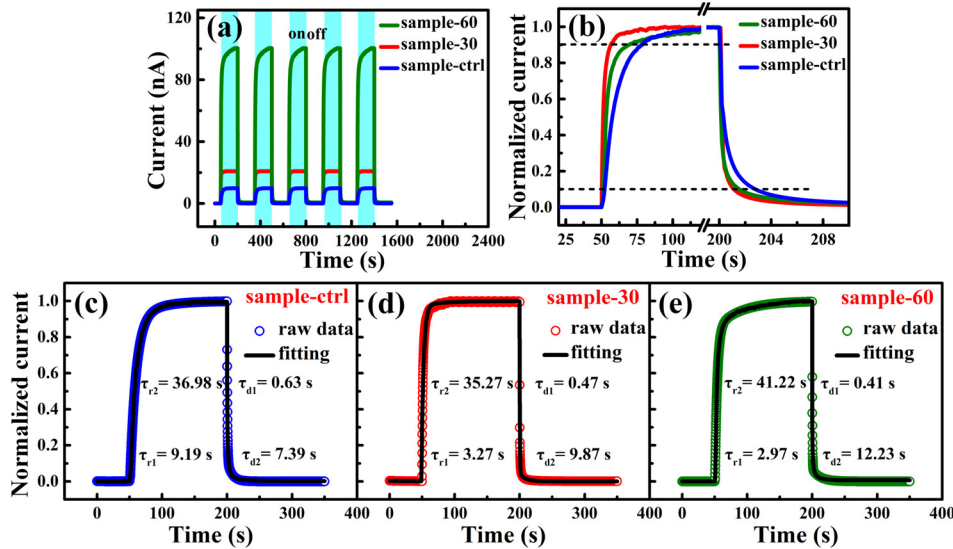


FIG. 6. Transient response of β -Ga₂O₃ MSM PDs: (a) response for multicycles, (b) normalized response for one single cycle; experimental data and fitted curves of the rise and decay processes for (c) sample-ctrl, (d) sample-30, and (e) sample-60. The light intensity was 34.7 μ W/cm², and the bias of the PD was 10 V.

Similarly, Kim *et al.* realized the oxygen-deficient and textured surface on the β -Ga₂O₃ substrate by metal-assisted chemical etching, and observed the dramatically enhanced responsivity of MSM PD.¹⁵

All the devices were reversibly modulated by UV-C illumination and demonstrated excellent reproducibility [Fig. 6(a)]. In most cases, the response time of PD is characterized by the decay time, τ_d (or rise time, τ_r), defined as the time during which the current drops from 90% to 10% (or increases from 10% to 90%) of the peak value.^{12,28,29} As shown in Fig. 6(b), the rise/decay times are 26.2 s/2.7 s, 6.3 s/1.1 s, and 18.0 s/1.6 s for sample-ctrl, sample-30, and sample-60, respectively. Clearly, the response speed can be effectively accelerated by the Ar-plasma pretreatment, although the effects vary for different plasma-generating powers. In order to further reveal the inner mechanisms, the transient response curves were fitted with a biexponential relaxation equation as follows:

$$I = I_0 + Ae^{\frac{-t}{\tau_1}} + Be^{\frac{-t}{\tau_2}}, \quad (2)$$

where I_0 is the steady-state photocurrent; t is the time; A and B are the constants; and τ_1 and τ_2 are the relaxation time constants corresponding to fast and slow components, respectively. The fast component is related to the electron transit time between electrodes, while the slow component is attributed to the excess lifetime of trapped carriers.^{8,12} The rise (τ_{r1}/τ_{r2}) and decay (τ_{d1}/τ_{d2}) time constants are listed in Table I. Apparently, the improved response speed was mainly attributed to the much shortened fast components (i.e., τ_{r1} and τ_{d1}) since the slow components (i.e., τ_{r2} and τ_{d2}) tended to be even longer. As explained in Fig. 5, our localized surface pretreatment substantially changed the M/S interfacial band bending, but did not affect the width of the whole depletion region (typically, more than several micrometers for unintentionally doped materials).^{17,30} It is different in the case of uniform heavy doping, including by V_o 's, in which the depletion-region width was much shortened, and thus the merit of quick drift velocity for carriers through this region was sacrificed.^{13,21} Therefore, the shortening of fast components could result from the facilitated rapid and direct tunneling of electrons at the M/S interface. In addition, the reduction in the RC time constant due to lower load

resistance might be another reason.³¹ On the other hand, the prolonging of slow components should be related to the higher V_o density in the near surface region of the β -Ga₂O₃ film, and thus more carrier trapping/detrapping at/near the M/S interface, which well explains the observed degradation in the response speed while increasing the plasma-generating power from 30 W to 60 W.

In summary, the low-energy Ar-plasma pretreatment was conducted selectively on the area of the β -Ga₂O₃ epitaxial film underneath the contacts of MSM PDs, leading to the localized oxygen deficiency. Both I_{dark} and I_{photo} were significantly increased, resulting in the dramatic improvement in sensitivity. The advantage of internal gain was preserved or became even larger. Even so, the response speed was much improved as well, which could be attributed to the rapid and direct tunneling of electrons at the M/S interface as well as the reduction in RC time constant. The pretreatment power and/or time can be further optimized to counterbalance the impacts of slow carrier-trapping/detrapping processes and the increase in I_{dark} . The experimental results demonstrate that the multiple performance characteristics can be simultaneously improved through the unique interface engineering in β -Ga₂O₃ solar-blind PDs.

See the [supplementary material](#) for additional device fabrication and measurements, XRD spectra, transmission spectra, AFM images, and I-V characteristics.

This work was supported by the National Natural Science Foundation of China under Contract No. 61504022 and the Fundamental Research Funds for the Central Universities under Grant No. ZYGX2018J026.

REFERENCES

- L. Sang, M. Liao, and M. Sumiya, *Sensors (Basel)* **13**(8), 10482 (2013).
- W. Zhang, J. Xu, W. Ye, Y. Li, Z. Qi, J. Dai, Z. Wu, C. Chen, J. Yin, and J. Li, *Appl. Phys. Lett.* **106**(2), 021112 (2015).
- Y. Hou, Z. Mei, H. Liang, C. Gu, and X. Du, *Appl. Phys. Lett.* **105**(13), 133510 (2014).
- D.-S. Tsai, W.-C. Lien, D.-H. Lien, K.-M. Chen, M.-L. Tsai, D. G. Senesky, Y.-C. Yu, A. P. Pisano, and J.-H. He, *Sci. Rep.* **3**, 2628 (2013).

- ⁵Z. Liu, F. Li, S. Li, C. Hu, W. Wang, F. Wang, F. Lin, and H. Wang, *Sci. Rep.* **5**, 14420 (2015).
- ⁶S. Pearnton, J. Yang, P. H. Cary, IV, F. Ren, J. Kim, M. J. Tadjer, and M. A. Mastro, *Appl. Phys. Rev.* **5**(1), 011301 (2018).
- ⁷R. Lin, W. Zheng, D. Zhang, Z. Zhang, Q. Liao, L. Yang, and F. Huang, *ACS Appl. Mater. Interfaces* **10**(26), 22419 (2018).
- ⁸A. Singh Pratiyush, S. Krishnamoorthy, S. Vishnu Solanke, Z. Xia, R. Muralidharan, S. Rajan, and D. N. Nath, *Appl. Phys. Lett.* **110**(22), 221107 (2017).
- ⁹M. Kim, J.-H. Seo, U. Singiseti, and Z. Ma, *J. Mater. Chem. C* **5**(33), 8338 (2017).
- ¹⁰K.-Y. Chen, C.-C. Hsu, H.-C. Yu, Y.-M. Peng, C.-C. Yang, and Y.-K. Su, *IEEE Trans. Electron Devices* **65**(5), 1817 (2018).
- ¹¹L.-X. Qian, H.-F. Zhang, P. Lai, Z.-H. Wu, and X.-Z. Liu, *Opt. Mater. Express* **7**(10), 3643 (2017).
- ¹²Y. Hou, Z. Mei, and X. Du, *J. Phys. D: Appl. Phys.* **47**(28), 283001 (2014).
- ¹³S. Cui, Z. Mei, Y. Zhang, H. Liang, and X. Du, *Adv. Opt. Mater.* **5**(19), 1700454 (2017).
- ¹⁴M. Heinemann, J. Berry, G. Teeter, T. Unold, and D. Ginley, *Appl. Phys. Lett.* **108**(2), 022107 (2016).
- ¹⁵M. Kim, H.-C. Huang, J. D. Kim, K. D. Chabak, A. R. K. Kalapala, W. Zhou, and X. Li, *Appl. Phys. Lett.* **113**(22), 222104 (2018).
- ¹⁶L.-X. Qian, Z.-H. Wu, Y.-Y. Zhang, P. T. Lai, X.-Z. Liu, and Y.-R. Li, *ACS Photonics* **4**(9), 2203 (2017).
- ¹⁷J. Carrano, T. Li, P. Grudowski, C. Eiting, R. Dupuis, and J. Campbell, *J. Appl. Phys.* **83**(11), 6148 (1998).
- ¹⁸E. Monroy, F. Omnès, and F. Calle, *Semicond. Sci. Technol.* **18**(4), R33 (2003).
- ¹⁹A. Sciuto, F. Roccaforte, S. Di Franco, V. Raineri, S. Billotta, and G. Bonanno, *Appl. Phys. Lett.* **90**(22), 223507 (2007).
- ²⁰S. Lany and A. Zunger, *Phys. Rev. B* **72**(3), 035215 (2005).
- ²¹D. Guo, Z. Wu, Y. An, X. Guo, X. Chu, C. Sun, L. Li, P. Li, and W. Tang, *Appl. Phys. Lett.* **105**(2), 023507 (2014).
- ²²Y. J. Tak, F. Hilt, S. Keene, W.-G. Kim, R. H. Dauskardt, A. Salleo, and H. J. Kim, *ACS Appl. Mater. Interfaces* **10**(43), 37223 (2018).
- ²³H. Jung, D. Kim, and H. Kim, *Appl. Surf. Sci.* **297**, 125 (2014).
- ²⁴J.-M. Lee, K.-M. Chang, S.-W. Kim, C. Huh, I.-H. Lee, and S.-J. Park, *J. Appl. Phys.* **87**(11), 7667 (2000).
- ²⁵J.-S. Park, J. K. Jeong, Y.-G. Mo, H. D. Kim, and S.-I. Kim, *Appl. Phys. Lett.* **90**(26), 262106 (2007).
- ²⁶J.-M. Lee, K.-K. Kim, S.-J. Park, and W.-K. Choi, *Appl. Phys. Lett.* **78**(24), 3842 (2001).
- ²⁷X. Gong, M. H. Tong, Y. J. Xia, W. Z. Cai, J. S. Moon, Y. Cao, G. Yu, C. L. Shieh, B. Nilsson, and A. J. Heeger, *Science* **325**(5948), 1665 (2009).
- ²⁸Y. Hou, Z. Mei, H. Liang, D. Ye, C. Gu, X. Du, and Y. Lu, *IEEE Trans. Electron Devices* **60**(10), 3474 (2013).
- ²⁹S. Oh, Y. Jung, M. A. Mastro, J. K. Hite, C. R. Eddy, Jr., and J. Kim, *Opt. Express* **23**(22), 28300 (2015).
- ³⁰G. Hu, C. Shan, N. Zhang, M. Jiang, S. Wang, and D. Shen, *Opt. Express* **23**(10), 13554 (2015).
- ³¹Z. Alaie, S. M. Nejad, and M. Yousefi, *Mater. Sci. Semicond. Process.* **29**, 16 (2015).